

Effect of Target Dynamics on Pharmacokinetics of a Novel Therapeutic Antibody against the Epidermal Growth Factor Receptor: Implications for the Mechanisms of Action

Jeroen J. Lammerts van Bueren,¹ Wim K. Bleeker,¹ Henrik O. Bøgh,³ Mischa Houtkamp,¹ Janine Schuurman,¹ Jan G.J. van de Winkel,^{1,2} and Paul W.H.I. Parren¹

¹Genmab BV; ²Immunotherapy Laboratory, Department of Immunology, University Medical Center Utrecht, Utrecht, the Netherlands; and ³Genmab A/S, Copenhagen, Denmark

Abstract

The epidermal growth factor receptor (EGFR) is overexpressed on many solid tumors and represents an attractive target for antibody therapy. Here, we describe the effect of receptor-mediated antibody internalization on the pharmacokinetics and dose-effect relationship of a therapeutic monoclonal antibody (mAb) against EGFR (2F8). This mAb was previously found therapeutically active in mouse tumor models by two dose-dependent mechanisms of action: blockade of ligand binding and induction of antibody-dependent cell-mediated cytotoxicity. *In vitro* studies showed 2F8 to be rapidly internalized by EGFR-overexpressing cells. *In vivo*, accelerated 2F8 clearance was observed in cynomolgus monkeys at low doses but not at high doses. This enhanced clearance seemed to be receptor dependent and was included in a pharmacokinetic model designed to explain its nonlinearity. Receptor-mediated clearance was also found to affect *in situ* antibody concentrations in tumor tissue. *Ex vivo* analyses of xenograft tumors of 2F8-treated nude mice revealed that relatively high antibody plasma concentrations were required for maximum EGFR saturation in high-EGFR-expressing human A431 tumors, in contrast to lower-EGFR-expressing human xenograft tumors. In summary, receptor-mediated antibody internalization and degradation provides a saturable route of clearance that significantly affects pharmacokinetics, particularly at low antibody doses. EGFR saturation in normal tissues does not predict saturation in tumor tissue as local antibody concentrations in EGFR-overexpressing tumors may be more rapidly reduced by antibody internalization. Consequently, antibody saturation of the receptor may be affected, thereby affecting the local mechanism of action. (Cancer Res 2006; 66(15): 7630-8)

Introduction

Fueled by technological advances enabling the accelerated development of humanized and fully human monoclonal antibodies (mAb), therapeutic mAbs have emerged as a rapidly expanding and increasingly important class of drugs (1). Most of these antibodies target human self-proteins and interfere with

processes critical to the pathology of the disease in question. Targeting of self-molecules may have a strong effect on mAb therapeutic application because the dynamics of the target molecule may significantly affect antibody pharmacokinetics and distribution. These aspects of passive antibody therapy have not been widely studied and are currently incompletely understood.

Characteristic for immunoglobulin G (IgG) is a relatively low clearance rate at low plasma concentrations and increased clearance at high concentrations. This effect is caused by saturation of the neonatal Fc receptor that rescues IgG molecules from degradation after cellular uptake (2–4). Therefore, it is remarkable that the reverse (i.e., a nonlinear clearance with enhanced kinetics at low dosing) has been observed by several investigators for a number of therapeutic antibodies, including those targeting epidermal growth factor receptor (EGFR), CD4, FAP, Her2, and CD11a (5–12). However, this phenomenon has not been observed for all therapeutic antibodies (13, 14) and seems to be associated with antibodies targeting cell surface-expressed self-molecules. Several investigators have proposed antibody internalization to be the cause of nonlinear clearance (5, 12, 15). Support for this idea comes from studies with labeled antibodies used for imaging or for targeting of cytotoxic agents (16–18). However, these latter studies were done at relatively low antibody dose. Therapies with labeled antibodies indeed are characterized by a high ratio of bound over free antibody; i.e., the antibody is present at non-saturating plasma concentrations and most antibody-conjugate is bound to target. Because naked antibodies generally cause less side effects than their drug/radiolabel-conjugated equivalents, therapy with naked antibodies is typically done at much higher mAb doses to achieve target saturation in the target tissue(s) and to engage all mechanisms of action. Therapies with naked antibodies therefore are characterized by a low ratio of bound over free antibody; i.e., the antibody is present at saturating plasma concentrations and most antibody is present in unbound state. Thus, the question remains to which extent antibody internalization may influence the pharmacokinetics and efficacy of passive antibody therapy.

Our previous studies have shown that 2F8 potently inhibits tumor growth in xenograft tumor models by engaging two possible therapeutic mechanisms of action (19). The first mechanism is blockade of EGFR signaling, which is most effective at receptor saturation, and therefore requires a relatively high antibody dose. Second, antitumor effects in mice were also observed at low 2F8 dose, corresponding to very low receptor occupancy. This latter effect is believed to particularly involve Fc receptor-mediated antibody-dependent cell-mediated cytotoxicity (ADCC). In the present study, we analyzed the effect of EGFR dynamics on the pharmacokinetic behavior of anti-EGFR 2F8 and its influence on local antibody concentrations. A pharmacokinetic model was

Note: Supplementary data for this article are available at Cancer Research Online (<http://cancerres.aacrjournals.org/>).

All authors are employees of Genmab.

Requests for reprints: Jan G.J. van de Winkel, Genmab B.V., Yalelaan 60, 3584 CM Utrecht, the Netherlands. Phone: 31-(0)-30-2-123-100; Fax: 31-(0)-30-2-123-110; E-mail: JWI@nl.genmab.com.

©2006 American Association for Cancer Research.
doi:10.1158/0008-5472.CAN-05-4010

developed to explain the observed nonlinear clearance of 2F8 in monkeys. Next, we did *in vitro* experiments with EGFR-expressing cells to examine the hypothesis that the accelerated clearance at low antibody doses is caused by receptor-mediated endocytosis and degradation, leading to antibody catabolism. Finally, we addressed the question of whether high EGFR overexpression may decrease interstitial antibody concentrations in solid tumors. Variations in levels of EGFR overexpression were shown to proportionally affect the rate of EGFR-mediated antibody consumption.

Materials and Methods

Antibodies. 2F8, a human IgG1 κ anti-EGFR mAb, has been generated and purified as described (19). Human IgG1 κ specific for keyhole limpet hemocyanin (KLH), developed using the same mouse strain, served as control. FITC-conjugated antibodies were prepared using a standard FITC labeling procedure (Pierce, Rockford, IL).

Monkey study designs. Two studies in cynomolgus monkeys (*Macaca fascicularis*) were conducted at Charles River Laboratories (Tranent, United Kingdom) in accordance with the Organization for Economic Cooperation and Development Principles of Good Laboratory Practice. The animals were of ages 14 to 23 months and weighed 2.0 to 3.2 kg. In the single-dose study, the animals were assigned to three treatment groups (one male and one female in each group) and received a single i.v. dose of 2, 20, or 40 mg/kg 2F8, respectively, followed by a 35-day post-dose observation period. In the multiple-dose study, the animals were assigned to four dose groups (six animals each), which on days 0, 7, 14, and 21 received i.v. administrations of 0, 2, 20, and 40 mg/kg 2F8, respectively. On completion of the last dose, the animals were kept for an additional 2-week observation period.

Mouse study design. Female nude BALB/c mice (*nu/nu*; 6-8 weeks old) were obtained from Charles River Laboratories (Maastricht, the Netherlands). Tumor xenografts were induced by s.c. inoculation of 5×10^6 A431 or SW480 cells or 10^7 BxPC-3 cells in the right flank. When tumors reached a volume of ~ 0.5 mL, mAbs were administered in a single i.p. dose. Two days later, mice were sacrificed and tumors cells analyzed for occupancy of EGFR by 2F8. Tumors were immersed in ice-cold fluorescence-activated cell sorting (FACS) buffer, cells were isolated through a cell-strainer and stained with anti-human IgG-FITC (with or without preincubation with saturating concentrations of 2F8) for FACS analyses. Furthermore, heparinized blood samples were taken from the retro-orbital plexus for determination of plasma 2F8 concentrations. EGFR occupancy with 2F8 of xenograft tumors was calculated from the mean fluorescence intensities (MFI) as a percentage of the maximum 2F8 occupancy using the formula $[(\text{MFI}_{\text{measured 2F8 occupancy}} - \text{background}) / (\text{MFI}_{\text{maximum 2F8 occupancy}} - \text{background})] \times 100\%$.

Pharmacokinetic analyses. A monoexponential curve fit was used to determine elimination half-life ($t_{1/2}$) of 2F8 pharmacokinetics in mice after a single i.p. dose. For the monkey studies, a different approach was chosen because monoexponential or biexponential curve fitting seemed to be inappropriate (see Supplementary data).

Cell lines. A431, SW480, and BxPC-3 cells were cultured in RPMI 1640 (BioWhittaker, Verviers, Belgium), supplemented with 10% heat-inactivated calf serum (Hyclone, Logan, UT), 50 IU/mL penicillin, 50 $\mu\text{g}/\text{mL}$ streptomycin, and, for BxPC-3, 2 mmol/L L-glutamine. Cells were detached using trypsin-EDTA treatment. For *in vivo* studies, subconfluent cells were tested for EGFR expression and *Mycoplasma* contamination before each experiment.

Antibody internalization analyzed by FACS. To determine cell surface-bound 2F8 at different time points, A431 cells were incubated with 20 $\mu\text{g}/\text{mL}$ 2F8 or 10 nmol/L epidermal growth factor (EGF)-biotin (Invitrogen, Carlsbad, CA) on ice for 30 minutes. Cells were rinsed thrice, split in two pools, and either warmed to 37°C to allow internalization or left on ice. Timed samples were taken in triplicates. Internalization was stopped by transferring cells to ice-cold FACS buffer. Cell surface-bound IgG was stained using rabbit anti-human IgG Fc γ F(ab')₂-FITC antibodies

(DAKO, Glostrup, Denmark). EGF-biotin was stained using phycoerythrin-conjugated streptavidin (DAKO) and samples were analyzed by FACS (BD FACSCalibur, Franklin Lakes, NJ). The 2F8 internalization rate, represented by the $t_{1/2}$ of the curve, was determined using one-phase exponential decay curve fitting.

Intracellular accumulation of 2F8 was measured by incubation of cells with FITC-conjugated 2F8 at 37°C or 4°C and timed samples were taken in triplicates. Fluorescence of extracellular-bound 2F8-FITC was quenched by addition of 2 mg/mL ethidium bromide (Fluka, Buchs, Switzerland) before acquisition. The 2F8-FITC internalization rate, defined as the internalization $t_{1/2}$ represented by doubling time of the intracellular FITC signal, was determined using one-phase exponential decay curve fitting.

Antibody internalization and lysosomal targeting analyzed by confocal microscopy. A431 cells were seeded in chamber slides and cultured overnight to attach. FITC-conjugated 2F8 or anti-KLH was added and incubated for 10 minutes, 4 hours, or 16 hours. Cells were placed on ice, rinsed with PBS, and fixed with 4% paraformaldehyde for 10 minutes. Cell membranes were stained with rhodamine-conjugated wheat germ agglutinin (WGA; Molecular Probes, Leiden, the Netherlands). Analyses were done using a Leica TCS NT confocal laser scanning microscope. Alternatively, cells were incubated with FITC-conjugated 2F8, as described above, and permeabilized with 0.1% saponin in PBS. Cells were incubated with noncompeting mouse anti-human EGFR mAb 528 (Merck, Nottingham, United Kingdom) to stain EGFR or with mouse antibodies against lysosome marker LAMP-1 (BD PharMingen, San Diego, CA). Next, cells were stained with tetramethylrhodamine-5-(and 6)-isothiocyanate (TRITC)-conjugated goat anti-mouse IgG (Beckman Coulter, Fullerton, CA) and analyzed using a Bio-Rad MRC 1000 Microscope with argon/krypton laser (Bio-Rad, Hercules, CA).

Catabolism of 2F8 by EGFR-overexpressing cells. A431 cells (1×10^5) were seeded in six-well plates and incubated overnight. Monolayers were incubated with FITC-conjugated 2F8 at 37°C (0-7 hours). Next, cells were rinsed with ice-cold PBS and lysed in nonreducing sample buffer (Invitrogen). Cell lysates were boiled, loaded on 4% to 15% acrylamide Tris-HCl SDS-PAGE gels (Bio-Rad), and run according to the instructions of the manufacturer.

Protein was transferred to nitrocellulose membranes (Bio-Rad) by Western blotting. Membranes were stained for the presence of FITC using rabbit anti-FITC antibodies (DAKO) and peroxidase-conjugated goat anti-rabbit IgG antibodies (Cell Signaling Technologies, Beverly, MA). Membranes were incubated with chemiluminescent substrate (Pierce). Chemiluminescence was measured using a GeneGnome imager and Genetools 3.06a software (Syngene, Cambridge, United Kingdom).

Saturation and biodistribution in monkeys. *In vivo* saturation levels of EGFR with 2F8 were studied by immunohistochemistry. Tissue sections were stained with or without preincubation with saturating concentrations of 2F8. FITC-conjugated monkey preabsorbed polyclonal sheep anti-human IgG antibodies and subsequent three-step method using peroxidase-conjugated streptavidin-biotin were used for detection of 2F8. Peroxidase activity was detected with diaminobenzidine. Differences in staining intensity indicated that receptor saturation for 2F8 binding was not achieved *in vivo*, whereas similar staining intensity indicated complete receptor saturation.

Statistical analyses. Data analyses were done using GraphPad Prism 4.01 software. Group data were reported as mean \pm SD.

Results

Enhanced *In vivo* Clearance of 2F8 at Low Plasma Concentrations via EGFR-Mediated Endocytosis of 2F8

Pharmacokinetic analyses. The potential effect of physiologic EGFR expression on pharmacokinetic behavior of 2F8 was studied in cynomolgus monkeys. 2F8 was raised against human EGFR and binds cynomolgus EGFR with similar avidity. The monkey study revealed a strong dose dependency of plasma clearance rates as shown in Fig. 1A. Clearance of 2F8 from plasma at doses of 2, 20,

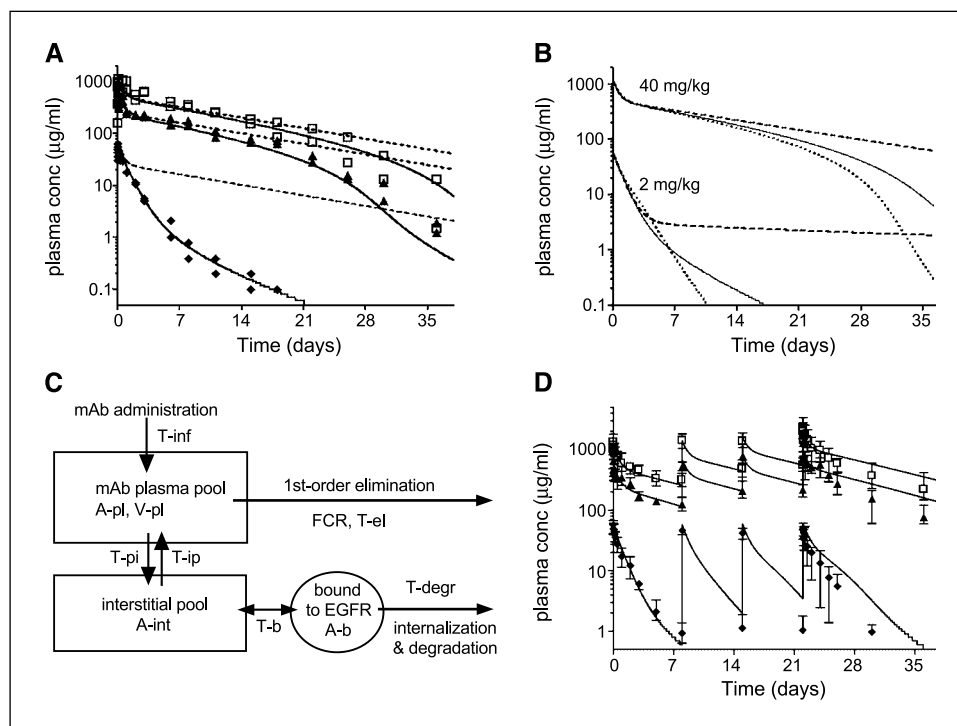


Figure 1. Pharmacokinetic model of 2F8 clearance in monkeys. **A**, plasma clearance of single dose of 2F8 in cynomolgus monkeys. 2F8 plasma concentrations are plotted on a log scale as a function of time after single i.v. doses of 2F8 at 2 (◆), 20 (▲), or 40 mg/kg (□). *Dashed lines*, expected clearance curves of human IgG using a two-compartment model, with plasma volume = 35 mL/kg, $k_{pi} = k_{ip} = -0.043 \text{ h}^{-1}$, and fractional catabolic rate = 0.0055 h^{-1} , which corresponds to an elimination $t_{1/2}$ of ~10 days. *Solid lines*, simulation of 2F8 clearance based on the “binding and elimination” model shown in (C) and further explained below. **B**, comparison of simulations of 2F8 plasma concentration after a single dose of 2 or 40 mg/kg by using three different approaches to model the saturable route of clearance: 1, Michaelis-Menten equation (*dotted lines*); 2, binding-only model (*dashed lines*); and 3, binding and elimination model (*solid lines*). All three models have the same basis: infused 2F8 is first distributed in a central plasma compartment of 35 mL/kg. From here, there is redistribution into an interstitial compartment with an apparent volume of 70 mL/kg, containing in equilibrium the same amount of IgG as the plasma pool. First-order elimination occurs from the plasma pool with a $t_{1/2}$ of 10 days. For the Michaelis-Menten model, 2F8 is in addition eliminated from the plasma pool via a saturable route described by the following equation: $V = (V_{\max} \times \text{concentration}) / (K_m + \text{concentration})$, in which V_{\max} is set at 0.07 mg/h and K_m at 5 µg/mL. For the binding-only model, there is no saturable elimination, but from the interstitial pool 2F8 binds reversibly to a compartment, which can fix a maximum of 2 mg/kg with half-maximal binding concentration of 1 µg/mL. For the binding and elimination model, bound 2F8 is eliminated with an elimination $t_{1/2}$ at 140 hours. **C**, schematic representation of the pharmacokinetic binding and elimination model used for the simulations of the monkey studies. It represents a plasma pool and an interstitial pool which equilibrates with the plasma pool. The first-order elimination occurs from the central plasma compartment with a certain $t_{1/2}$. Within the interstitial pool, a saturable clearance route is modeled by adding a binding compartment, representing EGFR-expressing cells, which equilibrates with the interstitial compartment. Bound 2F8 is eliminated with a certain $t_{1/2}$ by internalization/degradation. See Table 1 (see Supplementary data) for nomenclature. **D**, plasma clearance of multiple doses of 2F8 in monkeys. 2F8 plasma concentrations achieved after weekly i.v. dosing of 2F8 at 2 (◆), 20 (▲), or 40 mg/kg (□). *Solid lines*, simulated concentrations using the binding and elimination model with the same model variables as in (A and B).

and 40 mg/kg was 1.250, 0.270, and 0.225 mL/h/kg, respectively. In Fig. 1A, 2F8 plasma concentrations achieved after single i.v. dosing of 2, 20, or 40 mg/kg are plotted versus time. For comparison, we plotted the simulated time course based on the generally accepted “two-compartment model” for IgG clearance (20, 21) with linear kinetics in which $k_{pi} = k_{ip} = -0.043 \text{ h}^{-1}$, resulting in redistribution of ~50% of the i.v. injected antibody into the second compartment (interstitial space). A good fit for the initial phase after high-dose administration was obtained when plasma volume was set at 35 mL/kg and the fractional catabolic rate at 0.0055 h^{-1} , which corresponds to an elimination $t_{1/2}$ of ~10 days. The simulated biexponential time course in this model corresponded well with the clearance reported for a humanized anti-vascular endothelial growth factor (VEGF) mAb in monkeys (13). For 2F8, the predicted initial plasma concentrations corresponded reasonably well to concentrations achieved in monkeys treated at high dose (20 or 40 mg/kg) but, in contrast, diverged strongly at all low doses. Indeed, following a dose of 2 mg/kg, 2F8 levels declined rapidly towards plasma concentrations corresponding to concentrations 10 to 100 times below simulated values. Furthermore, after treatment at high doses, clearance accelerated when plasma

concentrations fell below concentrations of ~50 to 100 µg/mL. Monkeys treated with repeated doses of 2F8 also showed nonlinear clearance of 2F8 as shown in Fig. 1D. Clearance was faster after each 2 mg/kg dose than after each 20 or 40 mg/kg dose.

Primate anti-human antibody (PAHA) formation could not explain aberrant clearance of 2F8 because differences in clearance were observed immediately following administration, whereas PAHAs were only detected in a single low-dose animal and only appeared on day 21. To simulate pharmacokinetics of 2F8 more accurately, we first tried to describe the observed additional clearance using the Michaelis-Menten equation, as is frequently done in pharmacokinetic modeling. However, by applying this model, characterized by a maximum clearance level and a concentration at which half maximal clearance is obtained, we observed another deviation. The Michaelis-Menten model predicted a faster clearance at low antibody concentrations (e.g., 1 µg/mL in the low-dose treatment) than experimentally observed. Furthermore, it was not possible to find values for V_{\max} and K_m that fitted the observed clearance at both low and high doses.

We speculated that deviation from biexponential decay at low antibody concentrations might be mediated by binding of 2F8 to

EGFR located in tissues. To test this hypothesis, we determined clearance in mice, in which this binding component was absent (as 2F8 does not cross-react with murine EGFR; ref. 19). Consistent with the above, elimination $t_{1/2}$ observed in mice showed no accelerated clearance at low concentrations. In the time period from 5 hours to 21 days following i.p. administration of 2F8 in mice at a dose of 4 mg/kg, a monoexponential decay in plasma concentrations was observed. A $t_{1/2}$ of 8.8 ± 2.6 days (mean \pm SD; $n = 3$) was calculated for 2F8, which is within the expected range for human IgG in immunodeficient mice with low levels of plasma IgG (22). It was also close to the $t_{1/2}$ of 6.3 ± 0.9 days observed for a coadministered human isotype control mAb (anti-KLH; data not shown). In the absence of an EGFR-binding compartment, acceleration of clearance at low plasma concentrations was therefore not observed.

Next, we improved our initial model for simulating anti-EGFR clearance in monkeys by adding an additional saturable route of clearance, which is shown in Fig. 1C. To allow for binding of 2F8 in EGFR-expressing tissues, an additional compartment was added to the model, which results in a rapid but transient initial clearance after a low dose. In the absence of an elimination route, however, this did not predict acceleration of clearance after plasma concentrations dropped below 100 $\mu\text{g/mL}$ following treatment at high dose (Fig. 1B). Indeed, a much better prediction was obtained when a route of elimination was added to the binding compartment. This final model, including both a binding compartment with a B_{max} of 2 mg/kg and a rate constant for elimination by EGFR internalization and degradation (k_{deg}) of -0.005 h^{-1} ($t_{1/2} = 140$ hours), provided the best prediction for all experimental data taken together, both from single and multiple doses, as well as high- and low-dose treatment (Fig. 1A and D; Supplementary data). In one of the multiple 2 mg/kg dose animals, relatively high PAHA titers ($>1:800$) were detected after day 22 (Supplementary data), which may explain the large variation in observed concentrations in the last week in this group (Fig. 1D).

***In vitro* Internalization and Degradation of 2F8 by EGFR-Overexpressing Cells**

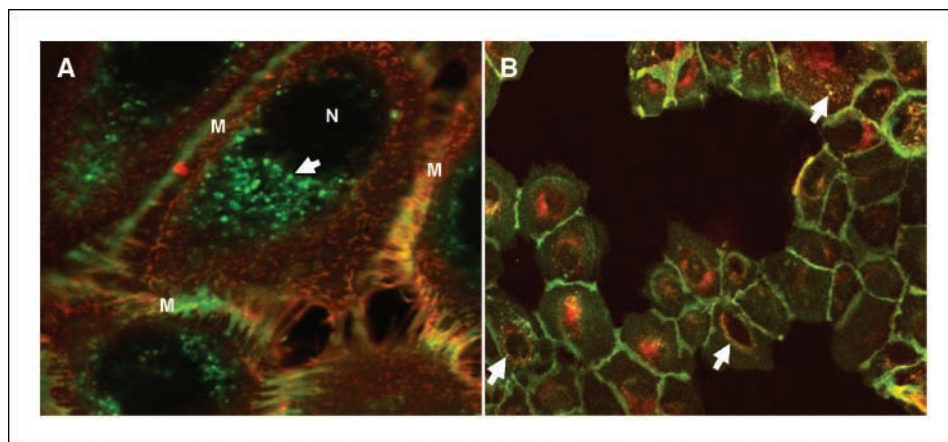
Our pharmacokinetic studies suggested that 2F8 internalization and degradation by EGFR-expressing cells may significantly influence its *in vivo* clearance and distribution. To obtain experimental evidence for such a mechanism, we investigated whether *in vitro* binding of 2F8 to EGFR resulted in internalization and mAb catabolism by EGFR-overexpressing cells.

After treating EGFR-overexpressing A431 cells with FITC-conjugated 2F8 for 1 hour, 2F8 was found at the cell membrane and in cytoplasmic microvesicles (Fig. 2A). Incubation of cells with a FITC-conjugated isotype control antibody showed no (sub)cellular staining (data not shown). Staining for EGFR in 2F8-FITC-treated cells showed colocalization of EGFR and 2F8 in cytoplasmic vesicles (Fig. 2B). In addition, EGFR not in complex with 2F8 was also found intracellularly. Membrane permeabilization by saponin made it difficult to observe colocalization at membrane surfaces, presumably because this structure was in part destroyed under these experimental conditions. Nonpermeabilized cells, however, clearly showed colocalization of both antibodies (data not shown). A control of permeabilized cells incubated with TRITC-conjugated goat anti-mouse IgG antibodies did not show any staining (not shown).

The EGFR-mediated internalization rate of 2F8 was quantified by flow cytometry. Measurements of cell surface-bound IgG on 2F8-incubated A431 cells showed a rapid decrease with time [$t_{1/2} = 18$ minutes; 95% confidence interval (95% CI), 11-43 minutes]. In control experiments, in which cells were incubated at 4°C, no decrease in cell-surface 2F8 was observed (Fig. 3A). In comparison, cells incubated with EGF-biotin showed a $t_{1/2}$ of 9 minutes (95% CI, 8-10 minutes; Fig. 3B), which is comparable with previous findings (23). Because decline of cell surface-bound 2F8 and EGF might in part be the result of dissociation, we also measured intracellular accumulation of FITC-conjugated 2F8. In addition to A431 cells, BxPC-3 and SW480 cells were tested, which have approximately 10 and 20 times lower EGFR expression levels than A431 cells, respectively (Fig. 3C).

To measure intracellular 2F8 accumulation, cells were incubated with 2F8-FITC at 4°C, and thereafter transferred to 37°C to allow internalization. Before FACS analyses, the fluorescence signal of extracellular 2F8-FITC was quenched with ethidium bromide. With this method, we were able to quench extracellular 2F8-FITC signals by 97% (data not shown). During incubation at 37°C, 2F8 rapidly accumulated intracellularly in all three cell lines (internalization $t_{1/2} = 10$ minutes; 95% CI, 8-11 minutes.). When cells were incubated with 2F8-FITC at 4°C, no intracellular accumulation of 2F8 was observed (Fig. 3D). Finally, because decrease of membrane-bound IgG may be caused by EGFR down-modulation, we determined EGFR cell-surface expression using the phycoerythrin-labeled non-cross-blocking mAb EGFR1. EGFR surface expression was shown not to be affected for all three cell lines during the course of the experiment (data not shown).

Figure 2. EGFR-mediated internalization of 2F8 by confocal microscopy. A431 cells were incubated for 1 hour with 2F8-FITC (green). A, cell membranes were stained with WGA-rhodamine (red). M and N, membranes and nuclei, respectively. EGFR located intracellularly in lysosome-like vesicles (white arrow). Magnification, $\times 1,000$. B, cells fixed with 4% paraformaldehyde, permeabilized with 0.1% saponin, and immunostained for EGFR (red). Yellow, colocalization. Incubation with 2F8 resulted in clustering of 2F8 in small vesicles containing EGFR (white arrows). Magnification, $\times 630$.



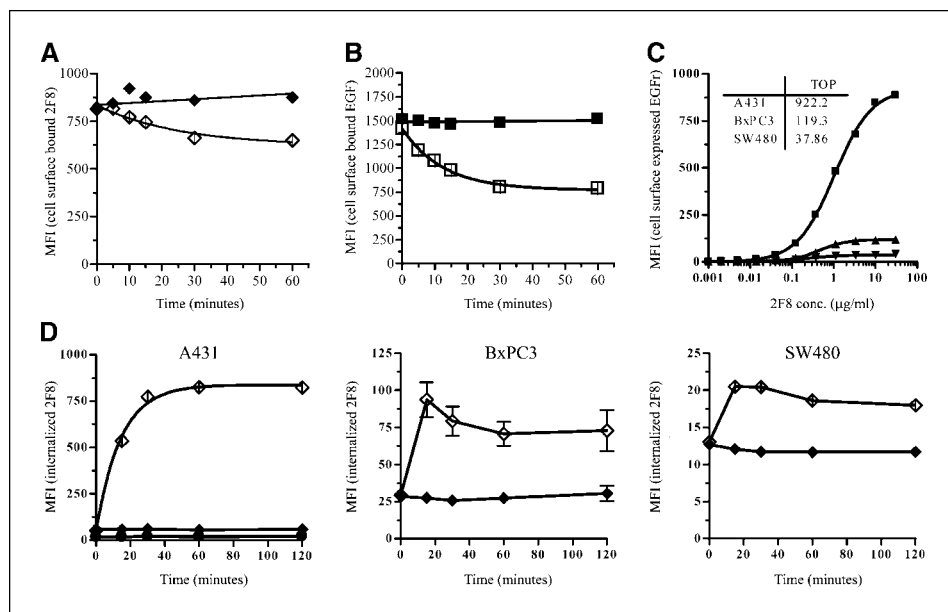


Figure 3. 2F8 internalization by EGFR-overexpressing cells. *A* and *B*, decrease of surface EGFR-bound 2F8 (*A*) or EGF (*B*) as detected by flow cytometry. Cells were labeled with 20 $\mu\text{g}/\text{mL}$ 2F8 (*A*; diamonds) or 10 nmol/L EGF (*B*; squares) at 4°C, washed, divided, and incubated at either 4°C (solid symbols) or 37°C (open symbols). Cell surface-bound 2F8 or EGF was then detected by FACS as described in Materials and Methods. *C*, cell-surface EGFR expression of A431, BxPC-3, and SW480 cell lines. EGFR expression levels on A431 (■), BxPC-3 (▲), and SW480 (▼) cells were measured by flow cytometry. Cells were incubated with serial dilutions of 2F8 and stained with FITC-conjugated F(ab)₂ fragments of rabbit anti-human IgG Fc and analyzed by FACS. *D*, intracellular accumulation of 2F8-FITC analyzed by flow cytometry. A431, BxPC-3, and SW480 cells were incubated with 20 $\mu\text{g}/\text{mL}$ 2F8-FITC at 4°C (◆) or 37°C (◇). Timed samples were drawn and internalized FITC-labeled mAb was specifically quantified in the presence of 2 mg/mL ethidium bromide, which quenches the fluorescence signal from the remaining cell surface-bound FITC-labeled mAb. An irrelevant FITC-labeled human antibody against KLH was used as an isotype control (●).

To assess whether receptor-mediated 2F8 internalization resulted in lysosomal degradation, we analyzed 2F8-FITC-incubated cells by confocal microscopy. Cells were labeled with 2F8-FITC and incubated at 37°C. After 4 or 20 hours, cells were stained for the lysosomal marker LAMP-1. At 4 hours, 2F8-FITC was evidently internalized and observed in small cytoplasmic vesicles, but colocalization with lysosomes was not yet observed. After 20 hours, however, colocalization of 2F8-FITC with lysosomal structures was shown (Fig. 4A).

Catabolism of 2F8 was examined by measuring 2F8 degradation by EGFR-overexpressing cells using Western blot analyses. Cell monolayers were incubated with 2F8-FITC for different time intervals and analyzed by immunoblotting using rabbit anti-FITC antibodies (Fig. 4B). The profiles shown are a graphical reproduction of the Western blot band profiles. Each line represents a lane on the blot. After 15 minutes, a similar profile was observed compared with a reference sample of 10 ng purified 2F8-FITC, indicating that no antibody degradation occurred. At later time

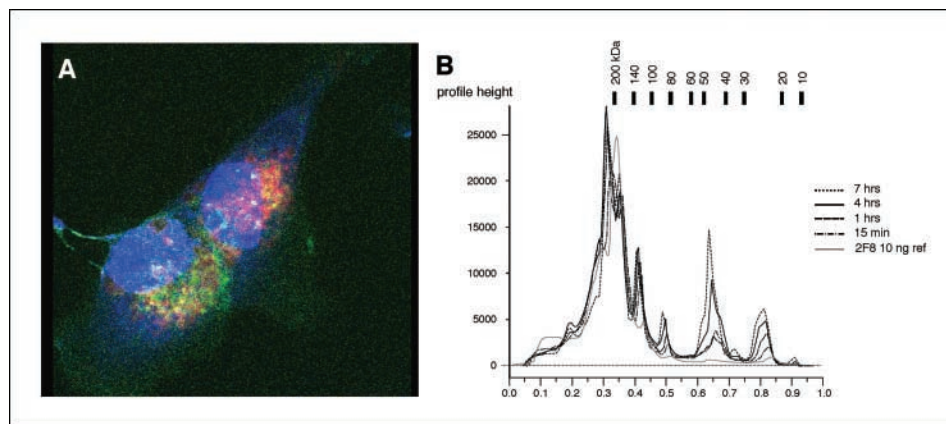
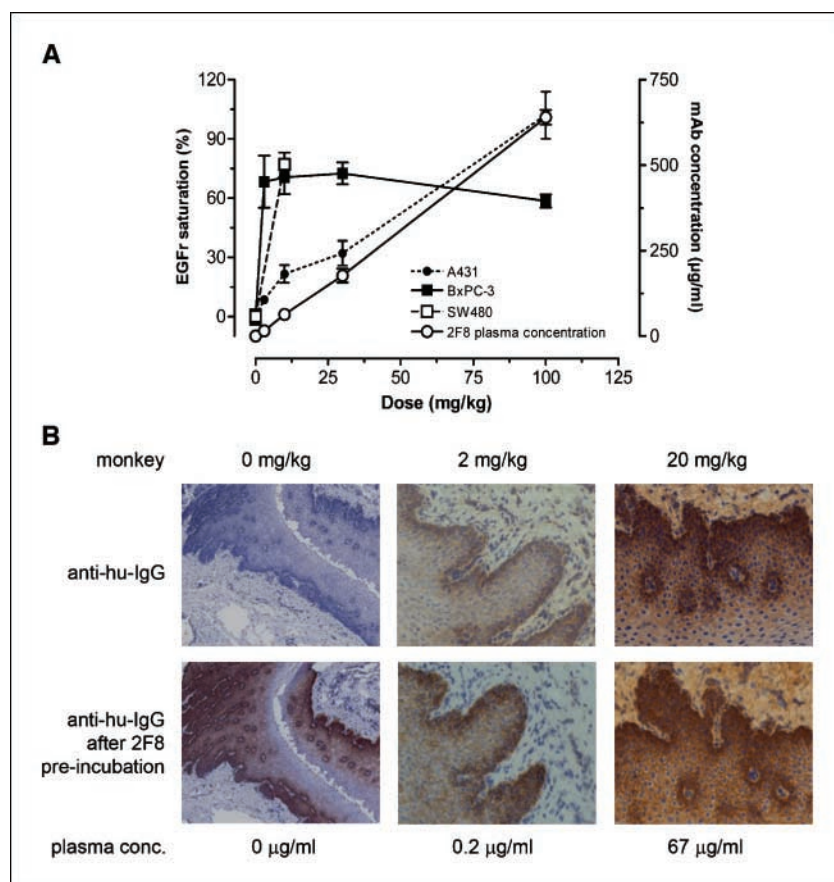


Figure 4. Lysosomal targeting of 2F8. *A*, A431 cells were labeled with 2F8-FITC (green) and incubated at 37°C for 20 hours. Cells were fixed with 4% paraformaldehyde, permeabilized, and immunostained for the lysosomal marker LAMP1 (red). Samples were then subjected to confocal microscopy. Yellow, colocalization of 2F8 and LAMP1. Nuclei are stained with 4',6-diamidino-2-phenylindole (blue). Magnification, $\times 1,000$. *B*, monolayers of A431 cells were incubated for 0 to 7 hours with 2F8-FITC. Cells were rinsed with ice-cold PBS, lysed in nonreducing sample buffer, and analyzed by SDS-PAGE followed by immunoblot. Purified 2F8-FITC was loaded as a control. The blot was stained with rabbit anti-FITC and goat anti-rabbit-horseradish peroxidase antibodies. A graphical reproduction of the Western blot banding profile is shown. Each line represents a lane on the blot. The signals are plotted as profile height versus distance traveled in the gel (Rf). An overlay of the Rf patterns is shown to illustrate the appearance of IgG fragments at different time points.

Figure 5. *In vivo* EGFR saturation of xenograft tumors and normal tissues with 2F8. **A**, 2F8 tissue saturation in xenograft tumors. Mice with either established BxPC-3 (—■—), SW480 (- - □ - -), or A431 (···●···) xenograft tumors were treated with a single dose of 2F8 (0, 3, 10, 30, or 100 mg/kg). Two days after dosing, tumors were removed for FACS analyses of EGFR saturation with 2F8. Points, mean EGFR saturations with 2F8 on isolated cells ($n = 4$), plotted against the left Y-axis; bars, SD. 2F8 plasma concentrations are plotted against the right Y-axis (—○—). **B**, tissue saturation and distribution in monkeys. Tissue biopsies were collected from monkeys treated with a single i.v. dose of 0, 2, or 20 mg/kg 2F8. Tissue biopsies of the pharynx were immunohistochemically stained for 2F8 using sheep anti-human IgG monkey preabsorbed antibodies (red-brown staining). *Top*, tissue distribution and dose-dependent staining of stratified epithelium-expressed EGFR by 2F8. *Bottom*, serial sections from the same tissue. These sections were preincubated with a saturating concentration of 2F8 to assess maximal staining. For morphologic interpretation, tissue sections were counterstained with hematoxylin.



points, IgG degradation products (FITC-conjugated peptide fragments of increasingly smaller size) accumulated in the cells.

EGFR Overexpression Influences Interstitial 2F8 Concentration in Xenograft Tumors

Previously, we showed a dose-dependent growth inhibition of xenograft tumors in athymic mice (19). For A431 tumors, we observed that an increase in 2F8 dose levels from 10 to 100 mg/kg showed increased tumor growth inhibition. *In vitro* studies showed that the maximum effect of 2F8 on A431 proliferation was reached at receptor saturation, suggesting that maximum receptor saturation was established in xenograft tumors only at the highest doses (100 mg/kg). We speculate that the high EGFR overexpression level of A431 cells, and relatively rapid internalization of 2F8, might influence local antibody concentrations in the tumors. To examine the effects of EGFR expression on 2F8 saturation in EGFR-(over)expressing tumors, we analyzed this in A431, BxPC-3, and SW480 xenograft tumors in athymic mice. 2F8 saturation analyses were done by flow cytometry 2 days after 2F8 treatment. Steady-state 2F8 distribution in xenograft tumors grown for 14 days was expected to be reached 1 day after i.p. administration, as earlier described by Wu et al. (13, 24, 25). As shown in Fig. 5A, 2F8 plasma concentrations required to saturate xenograft tumors were significantly higher for A431 tumors than for BxPC-3 and SW480 tumors. BxPC-3 xenograft tumors showed complete EGFR saturation at dose levels ~10 times lower than that for A431 xenograft tumors. For the low-EGFR-expressing SW480 xenograft tumors, 2F8 saturation was only determined for the 5 mg/kg dose, compared with saline control, and saturation was already achieved

at this low dose level. To study EGFR saturation in normal tissue, we analyzed skin tissue of 2F8-treated monkeys. EGFR is abundantly expressed in monkey epidermal tissue; however, EGFR expression is low compared with expression levels on A431 and BxPC-3 cells. In addition, normal tissue is more accessible to antibody in relation to normal tissue vascularization. Therefore, EGFR saturation was expected at lower 2F8 plasma concentrations, corresponding to saturating concentrations *in vitro*. Figure 5B shows that EGFR saturation in normal monkey tissue was established at doses between 2 and 20 mg/kg, corresponding to plasma concentrations <67 µg/mL 2F8.

Discussion

In this study, we obtained experimental evidence that 2F8 is internalized and degraded by EGFR-expressing cells. Furthermore, we showed that high EGFR expression levels in tumor xenografts result in reduced local 2F8 concentrations. Below, we discuss a pharmacokinetic model describing how binding, internalization, and degradation result in nonlinear clearance of 2F8, as observed in monkeys. Furthermore, we present a model explaining how, even at high mAb doses, target expression and dynamics may effect low local antibody concentrations in solid tumors.

First, we modeled 2F8 clearance in normal cynomolgus monkeys. Experimentally measured plasma concentrations were compared with a generally accepted two-compartment model for IgG clearance (20, 21) with linear kinetics. This revealed how 2F8 clearance deviated from the "linear clearance" behavior expected for IgG (i.e., a dose-independent clearance rate; refs. 21, 26).

Notably, we observed at high doses (20 and 40 mg/kg) acceleration of clearance when plasma concentrations fell below $\sim 100 \mu\text{g/mL}$. This indicated the presence of an additional route of clearance, which is negligible at higher plasma concentrations but becomes dominant at low 2F8 plasma concentrations. We hypothesized 2F8 also to be catabolized by EGFR-expressing cells in tissues, which may create an additional route of clearance. Elimination of anti-EGFR mAb by binding to tissues has been hypothesized as a significant clearance route for other anti-EGFR mAbs (e.g., cetuximab and hR3; refs. 8, 27, 28). For both mAbs, normal tissue uptake was highest in the liver and skin, where EGFR is highly expressed. Indeed, introduction of an additional saturable route of elimination in our initial two-compartment model provided a good prediction for all experimental data (both single and multiple doses). The best fit was obtained by modeling this saturable route by a reversibly bound 2F8 pool ($\sim 2 \text{ mg/kg}$) from which 2F8 is slowly eliminated ($t_{1/2} \sim 6 \text{ days}$).

In vitro studies with EGFR-overexpressing cells provided a biological substrate for our pharmacokinetic model. We obtained evidence that 2F8 is rapidly internalized and subsequently catabolized by EGFR-mediated internalization and lysosomal targeting. Flow cytometry data showed uptake of 2F8 to be proportional to the EGFR expression level of cells, resulting in high 2F8 uptake by high-EGFR-expressing A431 cells and proportionally lower uptake by low-EGFR-expressing BxPC-3 and SW480 cells. Remarkably, FACS analyses further showed that 2F8 intracellular accumulation reached equilibrium within 30 minutes (Fig. 3D). Under physiologic conditions, EGFR is internalized on ligand activation (29–31) and ligand-receptor complexes are targeted for lysosomal degradation attenuating signaling (32). A part of the internalized receptors is recycled to the cell surface (33). Interestingly, anti-EGFR mAb-induced down-modulation of EGFR was not observed during the 2-hour time period observed in the 2F8 internalization experiment, in contrast to what was previously

reported by Fan et al. (34, 35) for cetuximab. Possibly, EGFR surface expression can temporarily be replenished with EGFR present in the cell, but, finally, this process results in EGFR down-regulation (36, 37). Immunohistochemistry and Western blot analyses of 2F8-incubated cells confirmed that 2F8 was indeed catabolized by EGFR-expressing cells. The data suggest that EGFR-bound 2F8 was slowly routed for lysosomal degradation because, after 20 hours, not all intracellular 2F8 colocalized with lysosomes. This indicates degradation to be a much slower process than internalization.

Next, we addressed the question of whether in EGFR-over-expressing solid tumors, which are difficult to penetrate for large proteins such as antibodies (38), mAb concentrations could locally be influenced by receptor-mediated clearance. We therefore studied 2F8 biodistribution and EGFR saturation in xenograft tumors in mice. Because 2F8 does not cross-react to murine EGFR (19) and only binds to its cognate antigen expressed on xenografted tumor tissue, we assumed that tissue distribution of 2F8 would not be influenced by murine EGFR expression in tissues. Analyses of high-EGFR-overexpressing A431 xenografts showed low receptor saturation at 2F8 plasma concentrations that were sufficient for complete EGFR saturation in normal monkey tissues. This lack of saturation could not be readily explained as, even for large molecules such as mAb, equilibration and distribution into xenograft tumors was expected to be complete after the 2-day period (24, 25). It is also unlikely that competition of EGFR ligands with 2F8 binding could explain the low level of saturation, as in previous studies only a small fraction of xenograft-expressed EGFR occurred in its phosphorylated form, suggesting that only relatively low, subsaturating, ligand concentrations are present (19). This then suggests that the low saturation is due to low local 2F8 concentrations. Likely, the observed requirement for higher antibody dosing to achieve saturation in xenograft tumors compared with normal monkey tissue was caused by differences in EGFR dynamics, expression levels, and biodistribution kinetics.

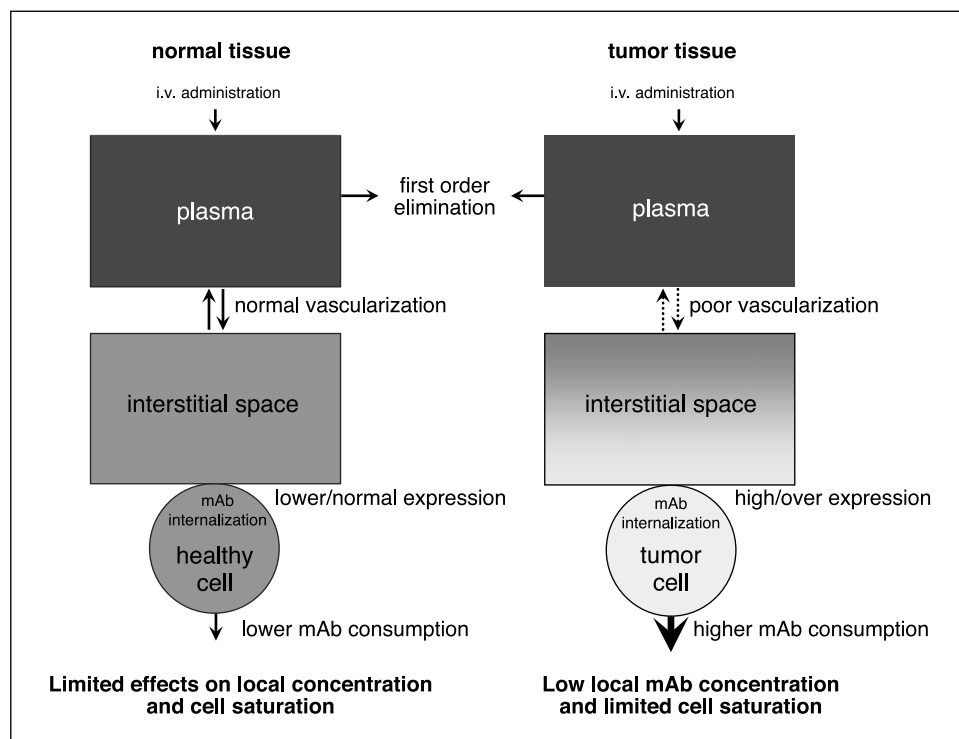


Figure 6. Target-mediated antibody pharmacokinetics and dose-effect relationship. The cartoon represents tissue distribution of mAb directed against EGFR in normal or tumor tissues (over)expressing the target antigen. Besides normal first-order clearance, self-antigen-directed mAbs are also catabolized in antigen-expressing tissues by target-mediated internalization. The gray levels indicate mAb concentration differences in each compartment. In normal tissue, a constant interstitial concentration of mAb is maintained by rapid vascular tissue distribution. Tumor tissue is characterized by aberrant vascularization. Therefore, mAb biodistribution relies, partly, on languid mAb diffusion. High mAb consumption by EGFR-(over)expressing cells creates low local mAb concentrations, which results in low receptor saturation. Clinical efficacy of therapeutic mAb relies on dose-dependent effector mechanisms. For optimal therapeutic effects, it is important that sufficient local mAb concentrations are achieved in tumor tissues to engage all potential mechanisms of action.

Although normal EGFR expression in monkey tissue is relatively low compared with EGFR overexpression in tumors, it still showed significant catabolism of 2F8, as shown by our pharmacokinetic experiments. However, this consumption of 2F8 could apparently be accommodated by rapid biodistribution of 2F8 into normal tissue, preventing the local interstitial concentrations to decrease. In contrast, biodistribution into solid tumors is much slower. It is known that tissue vascularization is immature in tumor tissues (39). Inadequate vascularization, physical hindrance of the collagen network in the tumor matrix, and elevated interstitial pressure result in delayed biodistribution of drugs (40). At low antibody doses, mAb affinity, intratumor diffusion rates, and clearance determine tumor penetration of antibodies (41). In high-dose treatment, characterized by a large excess of free antibody over bound antibody, affinity is expected to have a minor effect on tumor penetration. *In situ* analyses of high- and low-EGFR-expressing xenograft tumors indeed showed that EGFR saturation with 2F8 was related to EGFR-expression levels. We suggest that this phenomenon is best explained by a "sink model." The "sink" is created by a significant local consumption of mAb by internalization and degradation via its target. In combination with a low interstitial diffusion rate of mAb into the tumor, this sink results in low local mAb concentrations in the tumor. This hypothesis fits the observation that low-EGFR-expressing xenograft tumors show EGFR saturation with 2F8 at lower plasma concentrations than high EGFR-overexpressing tumors, due to a lower mAb-consuming sink. Taken together, this sink mechanism (Fig. 6) might influence the efficacy of anti-EGFR immunotherapy because only at complete receptor saturation with 2F8, both effector mechanisms (inhibition of EGFR signaling and ADCC) are predicted to be fully engaged. The model provides an explanation for our previous studies in which we observed significant tumor growth inhibition

of established A431 xenograft tumors in mice at 2F8 doses resulting in 15% to 30% saturation of tumor-expressed EGFR (10-30 mg/kg). We showed that this low-dose treatment was able to induce complete tumor regression in a moderately aggressive xenograft model. *In situ* analyses showed that EGFR phosphorylation was not inhibited, suggesting tumor growth inhibition was mainly caused by ADCC (19). Following high-dose treatment (100 mg/kg) in which saturation of tumor-expressed EGFR was achieved *in situ*, we observed complete inhibition of EGFR phosphorylation. Using an aggressive xenograft model, we observed that treatment efficacy augmented in parallel to EGFR saturation with 2F8.

In conclusion, we showed nonlinear clearance of 2F8 to be caused by binding of 2F8 to EGFR in tissues, followed by internalization and degradation. Inclusion of this mechanism in a pharmacokinetic model greatly improved the accuracy of simulations. Second, we conclude that local antibody concentrations in EGFR-(over)expressing solid tumors are reduced by antibody internalization, thereby affecting antibody saturation of the receptor. This is expected to influence the dose-effect relationship of anti-EGFR immunotherapies. It is important to take these considerations into account to optimize immunotherapy with anti-EGFR as well as therapeutic antibodies against other internalizing cell surface-expressed target molecules.

Acknowledgments

Received 11/8/2005; revised 5/29/2006; accepted 6/2/2006.

The costs of publication of this article were defrayed in part by the payment of page charges. This article must therefore be hereby marked *advertisement* in accordance with 18 U.S.C. Section 1734 solely to indicate this fact.

We thank G. Rigger, M. Pluyter, and T. Peeters for excellent technical assistance, and J. Gerritsen, G. Perdok, A. Vlug, S. Ruuls, and J. Oprins for their enthusiastic participation.

References

- Glennie MJ, van de Winkel JG. Renaissance of cancer therapeutic antibodies. *Drug Discov Today* 2003;8:503-10.
- Jungmans RP, Anderson CL. The protection receptor for IgG catabolism is the β 2-microglobulin-containing neonatal intestinal transport receptor. *Proc Natl Acad Sci U S A* 1996;93:512-6.
- Ober RJ, Radu CG, Ghetie V, Ward ES. Differences in promiscuity for antibody-FcRn interactions across species: implications for therapeutic antibodies. *Int Immunol* 2001;13:1551-9.
- Ghetie V, Ward ES. Transcytosis and catabolism of antibody. *Immunol Res* 2002;25:97-113.
- Baselga J, Pfister D, Cooper MR, et al. Phase I studies of anti-epidermal growth factor receptor chimeric antibody C225 alone and in combination with cisplatin. *J Clin Oncol* 2000;18:904-14.
- Mould DR, Davis CB, Minthorn EA, et al. A population pharmacokinetic-pharmacodynamic analysis of single doses of clenoliximab in patients with rheumatoid arthritis. *Clin Pharmacol Ther* 1999;66:246-57.
- Rowinsky EK, Schwartz GH, Gollob JA, et al. Safety, pharmacokinetics, and activity of ABX-EGF, a fully human anti-epidermal growth factor receptor monoclonal antibody in patients with metastatic renal cell cancer. *J Clin Oncol* 2004;22:3003-15.
- Robert F, Ezekiel MP, Spencer SA, et al. Phase I study of anti-epidermal growth factor receptor antibody cetuximab in combination with radiation therapy in patients with advanced head and neck cancer. *J Clin Oncol* 2001;19:3234-43.
- Bauer RJ, Dedrick RL, White ML, Murray MJ, Garovsky MR. Population pharmacokinetics and pharmacodynamics of the anti-CD11a antibody hu1L24 in human subjects with psoriasis. *J Pharmacokin Biopharm* 1999;27:397-420.
- Tokuda Y, Watanabe T, Omuro Y, et al. Dose escalation and pharmacokinetic study of a humanized anti-HER2 monoclonal antibody in patients with HER2/neu-overexpressing metastatic breast cancer. *Br J Cancer* 1999;81:1419-25.
- Kloft C, Graefe EU, Tanswell P, et al. Population pharmacokinetics of sibroutuzumab, a novel therapeutic monoclonal antibody, in cancer patients. *Invest New Drugs* 2004;22:39-52.
- Duconge J, Fernandez-Sanchez E, Macias A, et al. Monoclonal anti-EGFReceptor antibody (ior-R3) pharmacokinetic study in tumor bearing nude mice: role of the receptor-mediated endocytosis on drug clearance. *Eur J Drug Metab Pharmacokinet* 2002;27:101-5.
- Lin YS, Nguyen C, Mendoza JL, et al. Preclinical pharmacokinetics, interspecies scaling, and tissue distribution of a humanized monoclonal antibody against vascular endothelial growth factor. *J Pharmacol Exp Ther* 1999;288:371-8.
- Benincosa LJ, Chow FS, Tobia LP, et al. Pharmacokinetics and pharmacodynamics of a humanized monoclonal antibody to factor IX in cynomolgus monkeys. *J Pharmacol Exp Ther* 2000;292:810-6.
- Coffey GP, Stefanich E, Palmieri S, et al. *In vitro* internalization, intracellular transport, and clearance of an anti-CD11a antibody (Raptiva) by human T-cells. *J Pharmacol Exp Ther* 2004;310:896-904.
- Shih LB, Lu HH, Xuan H, Goldenberg DM. Internalization and intracellular processing of an anti-B-cell lymphoma monoclonal antibody, LL2. *Int J Cancer* 1994;56:538-45.
- Shockley TR, Lin K, Sung C, et al. A quantitative analysis of tumor specific monoclonal antibody uptake by human melanoma xenografts: effects of antibody immunological properties and tumor antigen expression levels. *Cancer Res* 1992;52:357-66.
- Coffey GP, Fox JA, Pippig S, et al. Tissue distribution and receptor-mediated clearance of anti-CD11a antibody in mice. *Drug Metab Dispos* 2005;33:623-9.
- Bleeker WK, Lammerts van Bueren JJ, van Ojik HH, et al. Dual mode of action of a human anti-epidermal growth factor receptor monoclonal antibody for cancer therapy. *J Immunol* 2004;173:4699-707.
- Waldmann TA, Strober W. Metabolism of immunoglobulins. *Prog Allergy* 1969;13:1-110.
- Morell A. Pharmacokinetics of intravenous immunoglobulin preparations. In: Strand V, editor. *Intravenous immunoglobulins in clinical practice*. 1st ed. New York (NY): Marcel Dekker; 1997. p. 1-18.
- Sell S, Fahey JL. Relationship between γ -globulin metabolism and low serum γ -globulin in germ-free mice. *J Immunol* 1964;93:81-7.
- Wiley HS, Herbst JJ, Walsh BJ, et al. The role of tyrosine kinase activity in endocytosis, compartmentation, and down-regulation of the epidermal growth factor receptor. *J Biol Chem* 1991;266:11083-94.
- Wu AM, Senter PD. Arming antibodies: prospects and challenges for immunoconjugates. *Nat Biotechnol* 2005;23:1137-46.
- Mattes MJ. Biodistribution of antibodies after intraperitoneal or intravenous injection and effect of carbohydrate modifications. *J Natl Cancer Inst* 1987;79:855-63.

26. Morell A, Terry WD, Waldmann TA. Metabolic properties of IgG subclasses in man. *J Clin Invest* 1970; 49:673–80.
27. Thomas SM, Grandis JR. Pharmacokinetic and pharmacodynamic properties of EGFR inhibitors under clinical investigation. *Cancer Treat Rev* 2004; 30:255–68.
28. Vallis KA, Reilly RM, Chen P, et al. A phase I study of ^{99m}Tc-hR3 (DiaCIM), a humanized immunoconjugate directed towards the epidermal growth factor receptor. *Nucl Med Commun* 2002;23:1155–64.
29. Carpenter G, Cohen S. 125I-labeled human epidermal growth factor. Binding, internalization, and degradation in human fibroblasts. *J Cell Biol* 1976;71:159–71.
30. Haigler HT, McKanna JA, Cohen S. Direct visualization of the binding and internalization of a ferritin conjugate of epidermal growth factor in human carcinoma cells A-431. *J Cell Biol* 1979;81:382–95.
31. van der Geer P, Hunter T, Lindberg RA. Receptor protein-tyrosine kinases and their signal transduction pathways. *Annu Rev Cell Biol* 1994;10:251–337.
32. Stoscheck CM, Carpenter G. Down-regulation of epidermal growth factor receptors: direct demonstration of receptor degradation in human fibroblasts. *J Cell Biol* 1984;98:1048–53.
33. Herbst JJ, Opreko LK, Walsh BJ, Lauffenburger DA, Wiley HS. Regulation of postendocytic trafficking of the epidermal growth factor receptor through endosomal retention. *J Biol Chem* 1994;269:12865–73.
34. Fan Z, Masui H, Altas I, Mendelsohn J. Blockade of epidermal growth factor receptor function by bivalent and monovalent fragments of 225 anti-epidermal growth factor receptor monoclonal antibodies. *Cancer Res* 1993;53:4322–8.
35. Fan Z, Lu Y, Wu X, Mendelsohn J. Antibody-induced epidermal growth factor receptor dimerization mediates inhibition of autocrine proliferation of A431 squamous carcinoma cells. *J Biol Chem* 1994;269:27595–602.
36. Burke PM, Wiley HS. Human mammary epithelial cells rapidly exchange empty EGFR between surface and intracellular pools. *J Cell Physiol* 1999;180:448–60.
37. Friedman LM, Rinon A, Schechter B, et al. Synergistic down-regulation of receptor tyrosine kinases by combinations of mAbs: implications for cancer immunotherapy. *Proc Natl Acad Sci U S A* 2005;102:1915–20.
38. Jain RK. Transport of molecules, particles, and cells in solid tumors. *Annu Rev Biomed Eng* 1999;1:241–63.
39. Hashizume H, Baluk P, Morikawa S, et al. Openings between defective endothelial cells explain tumor vessel leakiness. *Am J Pathol* 2000;156:1363–80.
40. Boucher Y, Baxter LT, Jain RK. Interstitial pressure gradients in tissue-isolated and subcutaneous tumors: implications for therapy. *Cancer Res* 1990;50:4478–84.
41. Graff CP, Wittrup KD. Theoretical analysis of antibody targeting of tumor spheroids: importance of dosage for penetration, and affinity for retention. *Cancer Res* 2003;63:1288–96.